Computational study of MHD mixed convective flow of Cu/Al_2O_3-water nanofluid in a porous rectangular cavity with slits, viscous heating, Joule dissipation and heat source/sink effects

N. Santhosh[1], R. Sivaraj,[1,2,*], V. Ramachandra Prasad[1] , O. Anwar Bég[3], Ho-Hon Leung[2], F. Kamalov[4] and S. Kuharat[3]

[1]Department of Mathematics, School of Advanced Sciences, Vellore Institute of Technology, Vellore 632014, India.
[2]Department of Mathematical Sciences, United Arab Emirates University, Al Ain, United Arab Emirates.
[3]Multi-Physical Engineering Sciences Group (MPESG), Aeronautical and Mechanical Engineering Department, School of Science, Engineering and Environment, University of Salford, Manchester M54WT, UK.
[4]Faculty of Engineering, Canadian University Dubai, Dubai, United Arab Emirates.

Emails: successofsanthosh@gmail.com; sivaraj.kpm@gmail.com; rcpmaths@gmail.com; O.A.Beg@salford.ac.uk; hohon.leung@uaeu.ac.ae; firuz@cud.ac.ae; S.Kuharat2@salford.ac.uk

Abstract

Heat transfer by means of mixed convection in enclosures is a topic of great interest due to several engineering and industrial applications including cooling systems of electronic components, building and thermal insulation systems, built-in-storage collectors, nuclear reactor systems, food storage, heat exchangers, solar collectors and materials processing. In view of these applications, the natural convective magnetohydrodynamic (MHD) flow and heat transfer inside a rectangular enclosure filled with porous media saturated with two different nanofluids is analysed in this study. The Tiwari -Das nanofluid model is adopted and two kinds of nanoparticles, namely aluminium oxide (Al_2O_3) and copper (Cu) nanoparticles with water base fluid are studied. The effects of magnetic field, viscous dissipation, Joule heating, and internal heat generation are incorporated in the model. Top and bottom walls of the enclosure are adiabatic with a constant temperature slit in the center of the walls. The vertical walls of the enclosure are adiabatic with a hot slit in the center of the walls. The robust, well-tested MAC (marker and cell) algorithm is used to numerically solve the transformed, dimensionless, nonlinear coupled two-dimensional momentum and energy conservation equations with carefully prescribed wall boundary conditions. The effect of pertinent parameters such as *Reynolds number (Re), Hartmann number (Ha), Eckert number (Ec), Richardson number (Ri), Darcy number (Da), Prandtl number (Pr), nanoparticle solid volume fraction (φ), and heat generation/absorption coefficient (Q)* on the Nusselt number, isotherm and streamline contour distributions in the enclosure is graphically displayed. With increment in volume fraction of nanoparticles, the flow, circulation, and temperature of the fluid inside the rectangular enclosure are increased. Internal heat generation also increases the rate of heat transfer. Magnetic field also strongly modifies the thermal characteristics. The simulations are relevant to hybrid fuel cells and nanomaterials processing.

Keywords: *Nanofluid, MHD, rectangular enclosure, viscous dissipation, Joule heating, heat absorption/generation, aluminium oxide (Al_2O_3) and copper (Cu) nanoparticles, MAC Method.*

1. Introduction

Nanofluids have received considerable attention in recent decades due to the enhanced thermophysical properties achieved by suspending the nanoparticles in the base fluids. Aluminium, copper, silver, and titanium are some popular metallic nanoparticles, whereas water, ethylene glycol, and oils are some of the most common examples of base fluids. Nanofluids have the potential to become the future of heat transfer fluids in a variety of thermal engineering applications including fuel cells, lubrication, surface coatings, biomedical devices, environmental remediation and electronic cooling systems. Hussain [1] elucidated that the nanomaterials may be helpful to increase the sensitivity, magnify the precision and improve the production limits in many industrial procedures. In addition, he inferred that the nanomaterials tend to provide green and sustainable solutions for several industrial developments. Many studies have revealed that nanofluids produce increased thermal conductivity and heat transfer rates due to the suspension of nanoparticles with high thermal conductivity in the base fluids with low thermal conductivity. Therefore, the nanofluids provide better thermal performance compared to conventional working fluids. This has mobilized considerable interest among researchers in the 21st century to analyse the possibilities of replacing the conventional heat transfer fluids with efficient nanofluids for various applications. Sivaraj and Santo Banerjee [2] highlighted some applications of non-Newtonian nanofluids and pointed out that the properties of nanofluids, such as thermal conductivity, viscosity and specific heat, are critical for elevating transport properties of nanofluids. Kavitha *et al.* [3] experimentally studied the heat transfer characteristics of a double pipe heat exchanger with different nanoparticle concentrations (volume fractions) of CuO-water nanofluid, noticing that nanofluids have a high potential to improve the heat transfer and are well suited to utilize for several realistic heat transfer tasks. Many studies have recently been conducted to examine the heat transfer efficiency of various nanofluids for enhancing as well as regulating the heat transfer in various processes. These have included both metallic and carbon-based nanoparticles. Bendrer *et al.* [4] performed numerical simulations with a Galerkin finite element method to study the features of convective hybrid nanofluid flow in wavy cubic enclosures, noting a strong acceleration with enhancing the Rayleigh-Darcy number.

The impact of an external static or oscillating magnetic field is very critical in a variety of industrial applications, including crystal growth, metal casting, smart functional coatings, controlling heat flux rates in liquid metal cooling blankets for fusion reactors. These applications feature fluent media which are electrically conducting and therefore can be

manipulated by external magnetic fields. To simulate such systems the science of magnetohydrodynamics (MHD) is required. Sheikholeslami *et al.* [5] numerically investigated the impact of magnetic field on natural convective flow of Al_2O_3–water nanofluid within a horizontal annulus between a heated triangular cylinder and its circular cylindrical enclosure by using the LBM approach. The results show that augmentations in the Hartmann number (magnetic body force number) induces a decrease in the Nusselt number. Javed *et al.* [6] performed a finite element numerical investigation of two-dimensional, laminar, steady MHD natural convective flow inside an isosceles triangular cavity filled with Cu-water nanofluid when the left wall is heated uniformly/non-uniformly by using the method. They found that in the uniform heating case the conduction dominates in the absence of magnetic field when Rayleigh number is kept small. In this case, an increase in Hartmann number reduces the strength of circulations and expands the curves of streamlines outwards, resulting in a straightening of curves along the side walls. Balla *et al.* [7] examined the effect of inclination angle of a cavity on magnetohydrodynamic natural convective flow and heat transfer in a square cavity containing a porous medium saturated with a nanofluid. They observed that as the magnetic parameter increases, the flow strength decreases. The augmentations in the strength of the magnetic field have a tendency to also increase the isotherm magnitudes. The Nusselt number decreases with increasing magnetic field parameter. Further industrial applications of magnetohydrodynamic flows include MHD energy generators, reactors, turbines, heat exchangers, and some power conversion devices. Furthermore, the impact of magnetic field in nanofluid enclosures is significant in batch processors, electromagnetic fuel cells and thermal process management, as noted in Sheikholeslami [8].

Natural convective flow in differentially heated enclosures containing Darcian or non-Darcian porous media saturated with fluids, has also stimulated considerable attention in the literature. This topic is of practical interest in several areas including hybrid fuel cells, filtration media for materials processing and also geothermal sciences. A porous medium offers a simple but effective mechanism for controlling transport phenomena in an enclosure geometry. Nithiarasu *et al.* [9] examined the effect of variable porosity on convective flow of a fluid inside a porous cavity. They found that the nature of porosity variation in the medium significantly affects the heat transfer and fluid flow. Mansour *et al.* [10] numerically studied the impact of entropy generation on natural convective flow of nanofluid in a square cavity saturated with porous media by using the finite volume method, observing that an increase in the Darcy number results in a decrease in the average total entropy generation and an increase in the average

Bejan number. Furthermore, they observed that the impact of viscous dissipation on average total entropy generation and average Bejan number is amplified with higher Darcy number (10^{-2}) whereas the impact of viscous dissipation on average entropy generation and average Bejan number is insignificant with lower Darcy number (10^{-4}). Reddy *et al.* [11] studied the natural convection Al_2O_3-water nanofluid flow and the heat transfer in a trapezoidal porous enclosure with a wavy bottom wall. They utilized the finite element method to solve the governing equations. The presence of porous medium was found to decelerates the nanofluid flow. In addition, they noticed from the sensitivity analysis that the average Nusselt number is more sensitive to the Darcy number. Sajjadi *et al.* [12] adopted the double MRT-LBM technique to investigate the natural convective flow of a copper-water nanofluid in a porous square cavity, noticing that variations in Darcy number strongly influence both fluid flow and temperature distribution. In addition, an increase in Darcy number improves the heat transfer rate and this effect is more pronounced at higher Rayleigh numbers. Al-Farhany *et al.* [13] investigated the influence of magnetic field on Fe_3O_4-water nanofluid flow within an inclined porous enclosure by using the finite element method. They showed that higher Darcy number (i. e. greater porous medium permeability), leads to a boost in the mean heat transfer rate.

In real viscous working fluids, encountered in manufacturing processes (e. g. nano-liquids), viscous dissipation arises in which mechanical energy is converted into heat. In magnetized liquids, Joule heating (also known as Ohmic dissipation) may also arise in systems where the magnetic field produces thermal dissipation effects. Both phenomena may contribute substantially towards heat transfer behaviour and are important to include in physico-mathematical models to provide a more realistic appraisal of transport characteristics. Neglection of these effects may lead to under-prediction in actual temperatures in real systems. The effect of viscous dissipation on thermal convection in a square cavity containing a saturated porous medium has been analysed by Badruddin *et al.* [14] using a finite element numerical approach. They noted that the local Nusselt number decreases with an increase in viscous dissipation parameter along the hot boundary (wall). However, the local Nusselt number increases with an increase in viscous dissipation parameter at the cold wall. They also identified that the difference between the average Nusselt number at a hot wall and cold wall increases with an increase in viscous dissipation parameter. Hossain *et al.* [15] have computed the unsteady, laminar, mixed convective heat transfer in a rectangular cavity in the presence of viscous dissipation. They deployed a finite difference method along with the successive over-relaxation (SOR) iteration technique. An increase in viscous dissipation parameter (Eckert

number) was observed to elevate the fluid temperature and resulted in the formation of vortex motion near the lower part of the cavity in an opposite direction to the central vortex. It was also shown that higher Eckert number resulted in augmenting the surface heat transfer rate from the top heated wall. Sheikholeslami *et al.* [16] investigated the viscous dissipation effect on Al_2O_3–water nanofluid flow and heat transfer in a square enclosure by using the control volume-based finite element method (CV-FEM). They used the Koo–Kleinstreuer–Li correlation to calculate the effective thermal conductivity and viscosity of the nanofluid. Their simulations showed that increasing the Eckert number decreases the Nusselt number. Ghalambaz *et al.* [17] investigated the effect of viscous dissipation on natural convection heat transfer in a square cavity filled with a nanofluid-saturated porous medium. They adopted the Buongiorno's mathematical model to characterise the nanofluid, elucidating that an increase in Eckert number boosts the temperature of the nanofluid and reduces the average Nusselt number at the hot wall. Swain *et al.* [18] used a fourth order Runge-Kutta method with shooting technique to simulate the stretching sheet magneto-convective flow in the presence of viscous dissipation and Joule heating effects, computing a significant modification in temperature distributions and rate of heat transfer to the wall with both dissipation effects. The numerical investigation of steady mixed convective flow and heat transfer in a lid-driven square cavity in the presence of heat-conducting obstacles and Joule heating effect is performed by Rahmann *et al*. [19]. They noticed that the Joule heating (Ohmic dissipation) has a significant effect on streamlines in the mixed convection and free convection dominated regions and also markedly modifies isotherms. An increase in Eckert number enhances the temperature of the fluid within the cavity. Mehmood *et al.* [20] investigated the effect of Joule heating on mixed convective alumina-water nanofluid flow in a square cavity containing an isothermally heated square blockage. They showed that increment in the Eckert number decreases the average Nusselt number and increases the average entropy generation. They also observed that the average temperature of the cavity increases with an increase in the Eckert number. The influence of Joule heating on the mixed convective hydromagnetic flow of an Al_2O_3–water nanofluid in a square enclosure was investigated by Dutta *et al.* [21]. An increase in Eckert number was found to raise temperature, diminish Nusselt number, and to increase the entropy generation. Furthermore, the effect of Joule heating was observed to be more pronounced with higher nanoparticle volume fraction values. Khan *et al.* [22] analysed the impact of viscous dissipation and Joule heating on nanoliquid boundary layer flow along an extending sheet, showing that higher dissipation effects notably decline the heat rate of heat transfer.

In many situations, heat is generated within a body by chemical, electrical or nuclear processes. A classic example from the nature for free convection caused by internal heat generation is motion in the atmosphere where heat is generated by absorption of sunlight. Most of the physical situations where the fluid and solid interaction takes place, notable temperature difference is observed between the surface of the solid body and ambient fluid. The knowledge of heat generation/absorption in moving fluids is important in view of several physical problems such as fluids undergoing exothermic and/or endothermic chemical reactions which finds applications in many areas of nuclear energy, fire and combustion modelling, etc. In materials processing "hot spots" or "thermal sinks" are also important as mechanisms of boosting or controlling temperature distributions in manufactured products. Kumar *et al.* [23] inferred that with higher values of heat absorption parameter, the regime is cooled. Prakash *et al.* [24] analysed the effect of heat sink parameter on mixed convective flow along an accelerated vertical wavy plate subject to varying temperature and mass diffusion. They found that magnifying the heat absorption parameter tends to absorb thermal energy which results in a decline in the temperature distribution. Mythili *et al.* [25] studied the impact of heat generation/absorption on viscoplastic thermal convection flow over a vertical cone and flat plate embedded in a non-Darcy porous medium. They noted that the heat transfer enhances with an increase in the heat source effect whereas it diminishes with a stronger heat sink effect. Hussain *et al.* [26] analysed the effect of volumetric heat generation/absorption on mixed convective flow of a nanofluid within a cavity by using the finite element method. They showed that significant adjustments are induced in heat transfer characteristics compared to the momentum characteristics with variation in internal heat generation/absorption effects. Sivasankaran *et al.* [27] examined the internal heat generation effect on convective flow of a nanofluid in an inclined porous cavity with the alternating direction implicit (ADI) method and inferred that flow acceleration is induced with increment in internal heat generation parameter which results in the enhancement of heat transfer. Further, they noticed that the weighted-average Nusselt number decreases with stronger heat generation. Tayebi *et al.* [28] used a finite volume technique to numerically simulate the impact of internal heat generation or absorption on natural convective flow of a copper-alumina/water hybrid nano-liquid in an annular cavity. They emphasized that internal heat generation/absorption strongly influences the thermal and flow field distributions, entropy generation distributions and heat transfer rate inside the annulus. Further, the maximum flow intensity occurs at a maximum internal heat generation value for the case of the conduction-dominated regime, while the maximum flow intensity

occurs in the presence of maximum internal heat absorption value for the case of the convection-dominated regime. Additionally, it was found that maximum rate of heat transfer occurs at a maximum heat absorption value.

To the best of the author's knowledge, to date, no work has been reported in the literature to analyse the transport of magnetohydrodynamic (MHD) Cu/Al_2O_3-water nanofluid flow in a rectangular porous enclosure with hot portions in the center of vertical walls constant temperature portions in the horizontal walls. Therefore, the objective of the present work is to investigate the *transport phenomena in MHD natural convective flow of two different nanofluids in the rectangular porous enclosure with slits in the presence of heat source/sink, viscous dissipation and Joule heating effects*. The Tiwari-Das model [29] is adopted to consider the properties of different nanofluids. A marker and cell (MAC) finite difference technique [30] is used to obtain computational solutions for the transformed, dimensionless, coupled nonlinear conservation equations. Results are visualized graphically for streamline, isotherm and local Nusselt number distributions. The simulations are relevant to emerging applications in magnetic materials processing [31], hybrid fuel cells [32-36] and magnetic heat exchangers exploiting nanofluids [37].

2. Mathematical Formulation

2.1 Governing equations

The figure schematically describes the two-dimensional geometry to be studied. Natural convective magnetohydrodynamic (MHD) flow and heat transfer in an electrically conducting nanofluid inside a rectangular enclosure with a bottom and top wall of length (*L*) and a right and left wall of height (*H*) is considered. The middle portions of the left and right walls are maintained at constant temperature T_h, while the middle portions of the top and bottom walls are maintained at constant temperature T_c. The temperature T_h is higher than the temperature T_c. The fluid flow in the rectangular enclosure is considered as unsteady, laminar and free convection. The enclosure contains an isotropic, homogenous, non-deformable porous medium and Darcy's law is employed. The Tiwari-Das nanofluid model is adopted to characterise the thermophysical properties. Two different nanofluids namely aluminium oxide-water and copper-water nanofluids are investigated. The flow field is influenced by a transversely applied magnetic field of strength B_0. The impact of viscous dissipation, Joule heating, and internal heat generation are taken into consideration. The magnetic nanofluid is dilute and there is local

thermal equilibrium between the nanoparticles and the aqueous base fluid. Hall current and magnetic induction effects are ignored.
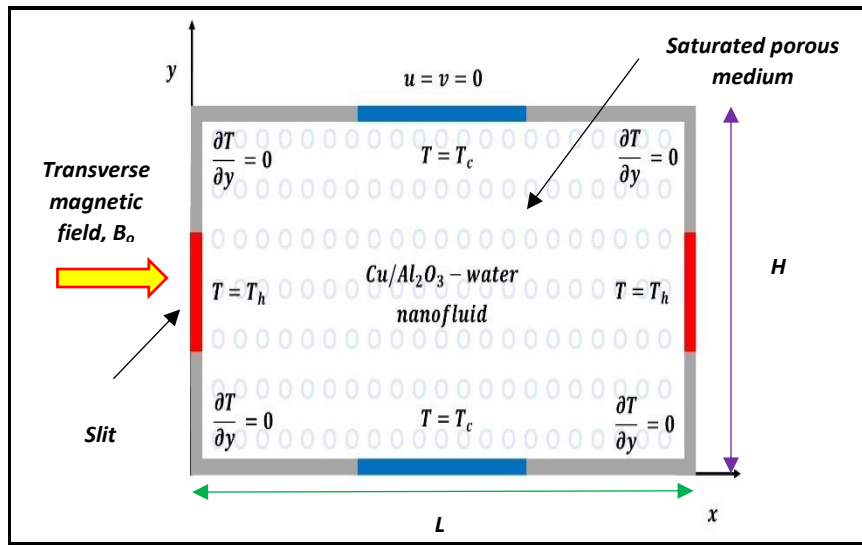

Figure 1: Flow configuration of the problem

In Cartesian coordinates, the governing equations for the regime i. e. the mass, momentum and energy conservation equations, may be expressed by extending the model in [11] to include porous drag, Joule heating, viscous dissipation and heat generation/absorption effects, as follows:

$$\frac{\partial u}{\partial x} + \frac{\partial v}{\partial y} = 0 \tag{1}$$

$$\frac{\partial u}{\partial t^*} + u\frac{\partial u}{\partial x} + v\frac{\partial u}{\partial y} = -\frac{1}{\rho_{nf}}\frac{\partial p}{\partial x} + \nu_{nf}\left[\frac{\partial^2 u}{\partial x^2} + \frac{\partial^2 u}{\partial y^2}\right] - \frac{\nu_{nf}}{K}u \tag{2}$$

$$\frac{\partial v}{\partial t^*} + u\frac{\partial v}{\partial x} + v\frac{\partial v}{\partial y} = -\frac{1}{\rho_{nf}}\frac{\partial p}{\partial y} + \nu_{nf}\left[\frac{\partial^2 v}{\partial x^2} + \frac{\partial^2 v}{\partial y^2}\right] - \frac{\nu_{nf}}{K}v - \frac{\sigma_{nf}B_0^2}{\rho_{nf}}v + \frac{(\rho\beta)_{nf}}{\rho_{nf}}g(T - T_c) \tag{3}$$

$$\frac{\partial T}{\partial t^*} + u\frac{\partial T}{\partial x} + v\frac{\partial T}{\partial y} = \frac{k_{nf}}{(\rho c_p)_{nf}}\left[\frac{\partial^2 T}{\partial x^2} + \frac{\partial^2 T}{\partial y^2}\right] + \frac{\sigma_{nf}B_0^2 v^2}{(\rho c_p)_{nf}} + \frac{\mu_{nf}}{(\rho c_p)_{nf}K}(u^2 + v^2)$$
$$+ \frac{\mu_{nf}}{(\rho c_p)_{nf}}\left(2\left(\frac{\partial u}{\partial x}\right)^2 + 2\left(\frac{\partial v}{\partial y}\right)^2 + \left(\frac{\partial v}{\partial x} + \frac{\partial u}{\partial y}\right)^2\right) + \frac{Q_0}{(\rho c_p)_{nf}}(T - T_c) \tag{4}$$

The following boundary conditions are prescribed at the enclosure walls:

On the left wall
$x = 0, 0 < y < 1, u = v = 0$
$\frac{\partial T}{\partial x} = 0, \quad for \quad 0 < y < \frac{L}{4}$
$T = T_h, \quad for \quad \frac{L}{4} < y < \frac{3L}{4} \tag{5}$
$\frac{\partial T}{\partial x} = 0, \quad for \quad \frac{3L}{4} < y < 1$

On the right wall

$x = 2, 0 < y < 1, u = v = 0$

$\frac{\partial T}{\partial x} = 0, \quad for \quad 0 < y < \frac{L}{4}$

$T = T_h, \quad for \quad \frac{L}{4} < y < \frac{3L}{4}$ (6)

$\frac{\partial T}{\partial x} = 0, \quad for \quad \frac{3L}{4} < y < 1$

On the top wall

$y = 1, 0 < x < 2, u = v = 0$

$\frac{\partial T}{\partial y} = 0, \quad for \quad 0 < x < \frac{L}{4}$

$T = T_c, \quad for \quad \frac{L}{4} < x < \frac{3L}{4}$ (7)

$\frac{\partial T}{\partial y} = 0, \quad for \quad \frac{3L}{4} < x < 2$

On the bottom wall

$y = 0, 0 < x < 2, u = v = 0$

$\frac{\partial T}{\partial y} = 0, \quad for \quad 0 < x < \frac{L}{4}$

$T = T_c, \quad for \quad \frac{L}{4} < x < \frac{3L}{4}$ (8)

$\frac{\partial T}{\partial y} = 0, \quad for \quad \frac{3L}{4} < x < 2$

2.2. Thermophysical properties of nanofluids:

The thermal and physical properties of nanofluids are important for improving the thermal performance of the working fluid. The physical and thermal properties of nanofluids are considered as follows based on the Tiwari-Das nanoscale model [29] which uses the Maxwell and Brinkmann models:

Density of the nanofluid:

$$\rho_{nf} = (1 - \varphi)\rho_f + \varphi\rho_p \tag{9}$$

Heat capacitance of the nanofluid:

$$(\rho C_p)_{nf} = (1 - \varphi)(\rho C_p)_f + \varphi(\rho C_p)_p \tag{10}$$

Thermal expansion coefficient of the nanofluid:

$$(\rho\beta)_{nf} = (1 - \varphi)(\rho\beta)_f + \varphi(\rho\beta)_p \tag{11}$$

Thermal diffusivity of the nanofluid is defined by:

$$\alpha_{nf} = \frac{k_{nf}}{(\rho C_p)_{nf}} \tag{12}$$

The thermal conductivity of the nanofluid is:

$$\frac{k_{nf}}{k_f} = \frac{(k_p + 2k_f) - 2\varphi(k_f - k_p)}{(k_p + 2k_f) + \varphi(k_f - k_p)} \tag{13}$$

The dynamic viscosity of the nanofluid is:

$$\mu_{nf} = \frac{\mu_f}{(1 - \varphi)^{2.5}} \tag{14}$$

Electrical conductivity of the nanofluid:

$$\frac{\sigma_{nf}}{\sigma_f} = \left[1 + \frac{3(\gamma-1)\varphi}{(\gamma+2)-(\gamma-1)\varphi}\right] \text{ where } \gamma = \frac{\sigma_p}{\sigma_f} \tag{15}$$

Table 1: Thermophysical properties of water and nanoparticles: [10, 11]

Property	Water	Al_2o_3	Cu
$\rho(kgm^{-3})$	997.1	3970	8,933
$C_p(Jkg^{-1}K^{-1}$	4179	765	385
k($Wm^{-1}k^{-1}$)	0.613	40	401
$\beta(k^{-1})$	21×10^{-5}	0.85×10^{-5}	1.67×10^{-5}
$\sigma(\Omega^{-1}m^{-1})$	0.05	1×10^{-10}	5.96×10^7
μ (Pa.s)	9.09×10^{-4}	-	-

2.3 Transformation of Model

To reduce the equations (1)– (4) into non-dimensional forms, the following non-dimensional quantities are introduced:

$$X = \frac{x}{L}; Y = \frac{y}{L}; t = \frac{t^*U_0}{L}; U = \frac{u}{U_0}; V = \frac{v}{U_0}; P = \frac{p}{\rho_f U_0^2}; \theta = \frac{T-T_c}{T_h-T_c} \tag{16}$$

In dimensionless form, the governing equations by virtue of Eqn. (16) emerge as follows:

$$\frac{\partial U}{\partial X} + \frac{\partial V}{\partial Y} = 0 \tag{17}$$

$$\frac{\partial U}{\partial t} + U\frac{\partial U}{\partial X} + V\frac{\partial U}{\partial Y} = -\left(\frac{\rho_f}{\rho_{nf}}\right)\frac{\partial P}{\partial X} + \left(\frac{\nu_{nf}}{\nu_f}\right)\frac{1}{Re}\left[\frac{\partial^2 U}{\partial X^2} + \frac{\partial^2 U}{\partial Y^2}\right] - \left(\frac{\nu_{nf}}{\nu_f}\right)\frac{1}{Re\,Da}U \tag{18}$$

$$\frac{\partial V}{\partial t} + U\frac{\partial V}{\partial X} + V\frac{\partial V}{\partial Y} = -\left(\frac{\rho_f}{\rho_{nf}}\right)\frac{\partial P}{\partial Y} + \left(\frac{\nu_{nf}}{\nu_f}\right)\frac{1}{Re}\left[\frac{\partial^2 V}{\partial X^2} + \frac{\partial^2 V}{\partial Y^2}\right] - \left(\frac{\nu_{nf}}{\nu_f}\right)\frac{1}{Re\,Da}V -$$
$$\left(\frac{\rho_f}{\rho_{nf}}\right)\left(\frac{\sigma_{nf}}{\sigma_f}\right)\frac{Ha^2}{Re}V + \frac{(\rho\beta)_{nf}}{\rho_{nf}\beta_f}\,Ri\,\theta \tag{19}$$

$$\frac{\partial \theta}{\partial t} + U\frac{\partial \theta}{\partial X} + V\frac{\partial \theta}{\partial Y} = \left(\frac{\alpha_{nf}}{\alpha_f}\right)\frac{1}{Re\,Pr}\left[\frac{\partial^2 \theta}{\partial X^2} + \frac{\partial^2 \theta}{\partial Y^2}\right] + \left(\frac{\mu_{nf}}{\mu_f}\right)\left(\frac{(\rho C_p)_f}{(\rho C_p)_{nf}}\right)\frac{Ec}{Da\,Re}(U^2 + V^2) +$$
$$\left(\frac{\sigma_{nf}}{\sigma_f}\right)\left[\frac{(\rho C_p)_f}{(\rho C_p)_{nf}}\right]\frac{Ha^2\,Ec}{Re}V^2 + \left(\frac{\mu_{nf}}{\mu_f}\right)\left(\frac{(\rho C_p)_f}{(\rho C_p)_{nf}}\right)\frac{Ec}{Re}\left(2\left(\frac{\partial U}{\partial X}\right)^2 + 2\left(\frac{\partial V}{\partial Y}\right)^2 + \left(\frac{\partial V}{\partial X} + \frac{\partial U}{\partial Y}\right)^2\right) +$$
$$\left(\frac{\alpha_{nf}}{\alpha_f}\right)\frac{Q}{Re\,Pr}\theta \tag{20}$$

Here *X, Y* are dimensionless coordinates, *t* is dimensionless time, *U,V* are dimensionless velocity components in the *X, Y* directions, *P* is dimensionless pressure, θ is dimensionless temperature, $Pr = \frac{\nu_f}{\alpha_f}$ is the Prandtl number, $Ha = B_0 L\sqrt{\frac{\sigma_f}{\mu_f}}$ is the Hartmann number (magnetic body force parameter), $Gr = \frac{g\beta_f(T_h-T_c)H^3}{\nu_f^2}$ is the Grashof number (thermal buoyancy parameter), $Da = \frac{K}{H^2}$ is the Darcy number (dimensionless permeability), $Ec = \frac{U_0^2}{(C_p)_f(T_h-T_c)}$ is

the Eckert number (viscous dissipation parameter), $Re = \frac{v_f}{U_0 L}$ is the Reynolds number (based on the enclosure $Ri = \frac{Gr}{Re^2}$ is the Richardson number and $Q = \frac{Q_0 L^2}{(\rho C_p)_f \alpha_f}$ is the Heat generation/absorption coefficient.

The dimensionless forms of the boundary conditions are as follows:

On the left wall
$X = 0, 0 < Y < 1, U = V = 0$
$\frac{\partial \theta}{\partial X} = 0, for\ 0 < Y < \frac{1}{4}$
$\theta = 1, for\ \frac{1}{4} < Y < \frac{3}{4}$ $\qquad\qquad$ (21)
$\frac{\partial \theta}{\partial X} = 0, for\ \frac{3}{4} < Y < 1$

On the right wall
$X = 2, 0 < Y < 1, U = V = 0$
$\frac{\partial \theta}{\partial X} = 0, for\ 0 < Y < \frac{1}{4}$
$\theta = 1, for\ \frac{1}{4} < Y < \frac{3}{4}$ $\qquad\qquad$ (22)
$\frac{\partial V}{\partial X} = 0, for\ \frac{3}{4} < Y < 1$

On the top wall
$Y = 1, 0 < X < 2, U = V = 0$
$\frac{\partial \theta}{\partial y} = 0, for\ 0 < X < \frac{2}{4}$
$\theta = 1, for\ \frac{2}{4} < X < \frac{6}{4}$ $\qquad\qquad$ (23)
$\frac{\partial \theta}{\partial y} = 0, for\ \frac{6}{4} < X < 2$

On the bottom wall
$Y = 0, 0 < X < 2, U = V = 0$
$\frac{\partial \theta}{\partial Y} = 0, for\ 0 < X < \frac{2}{4}$
$\theta = 1, for\ \frac{2}{4} < X < \frac{6}{4}$ $\qquad\qquad$ (24)
$\frac{\partial \theta}{\partial Y} = 0, for\ \frac{6}{4} < X < 2$

2.4 Engineering quantities

Nusselt number:
The local Nusselt number is given by the following expression
$$Nu = -\frac{k_{nf}}{k_f}\left(\frac{\partial \theta}{\partial Y}\right)_{Y=0} \qquad\qquad (25)$$

3. MAC solution and validation

The momentum and energy equations (18) – (20) with the associated boundary conditions (21)-(24) are strongly nonlinear and have been solved by adopting the marker and cell (MAC) finite

difference method [30]. The pressure distribution is obtained by making use of the continuity equation (17). The numerical solutions are generated in terms of velocity components (u, v) which represent U, V in the differential equations. The X, Y coordinates are represented by (x,y) in the MAC algorithms. In the MAC approach, although viscous flow is considered, viscosity is not required for numerical solutions. Cell boundaries are labelled with half-integer values based on the finite-difference discretization method. Appropriate details of the numerical discretization procedure is discussed in this section. According to the *weak conservation* form of the modified unsteady two-dimensional Navier-Stokes equations and the temperature equation as described by eqns. (1) – (4), a grid meshing procedure is implemented using the following notation at the centre of the cells:

$$u_{i-\frac{1}{2},j} = \frac{1}{2}\left(u_{i-1,j} + u_{i,j}\right). \tag{26}$$

Here, the subscripts i and j in the previous inequality represent space coordinated in the X and Y directions, respectively.

Applying Eqn. (26) into the X-momentum conservation Eqn. (18), leads to the following:

Discretized advection terms:

$$\frac{\partial(uu)}{\partial x} = \frac{uu_1 - uu_2}{\Delta x}. \tag{27}$$

Here,

$$uu_1 = \left(\frac{1}{2}\left(u_{i,j} + u_{i+1,j}\right)\right)^2. \tag{28}$$

$$uu_2 = \left(\frac{1}{2}\left(u_{i-1,j} + u_{i,j}\right)\right)^2. \tag{29}$$

Consequently:

$$\frac{\partial(uv)}{\partial y} = \frac{uv_1 - uv_2}{\Delta y}. \tag{30}$$

Here,

$$uv_1 = \frac{1}{2}\left(u_{i,j} + u_{i,j+1}\right).\frac{1}{2}\left(v_{i,j} + v_{i+1,j}\right). \tag{31}$$

$$uv_2 = \frac{1}{2}\left(u_{i,j} + u_{i,j-1}\right).\frac{1}{2}\left(v_{i,j-1} + v_{i+1,j-1}\right). \tag{32}$$

For *second-order* derivatives, the following *central difference* formulae are used:

$$\nabla^2 u = \frac{\partial^2 u}{\partial x^2} + \frac{\partial^2 u}{\partial y^2}. \tag{33}$$

$$\nabla^2 u = \frac{u_{i-1,j} - 2u_{i,j} + u_{i+1,j}}{\Delta x^2} + \frac{u_{i,j-1} - 2u_{i,j} + u_{i,j+1}}{\Delta y^2}. \tag{34}$$

Applying Eqn. (26) in the Y-direction momentum conservation Eqn. (19) one obtains the following:

Advection term:

$$\frac{\partial(vu)}{\partial x} = \frac{vu_1 - vu_2}{\Delta x}. \tag{35}$$

The following notations are used in this method:

$$uv_1 = \frac{1}{2}(u_{i,j+1} + u_{i,j}).\frac{1}{2}(v_{i,j} + v_{i+1,j}). \tag{36}$$

$$uv_2 = \frac{1}{2}(u_{i-1,j+1} + u_{i-1,j}).\frac{1}{2}(v_{i,j} + v_{i-1,j}). \tag{37}$$

$$\frac{\partial(vv)}{\partial y} = \frac{vv_1 - vv_2}{\Delta y}. \tag{38}$$

$$vv_1 = \left(\frac{1}{2}(v_{i,j+1} + v_{i,j})\right)^2. \tag{39}$$

$$vv_2 = \left(\frac{1}{2}(v_{i,j-1} + v_{i,j})\right)^2. \tag{40}$$

The central difference formulae for the Laplacian operators are defined by:

$$\nabla^2 v = \frac{\partial^2 v}{\partial x^2} + \frac{\partial^2 v}{\partial y^2}. \tag{41}$$

$$\nabla^2 v = \frac{v_{i-1,j} - 2v_{i,j} + v_{i+1,j}}{\Delta x^2} + \frac{v_{i,j-1} - 2v_{i,j} + v_{i,j+1}}{\Delta y^2}. \tag{42}$$

The *X*-momentum equation discretization approach takes the form:

$$\bar{U} = U^n + dt\left\{-\left(U\frac{\partial U}{\partial X} + V\frac{\partial U}{\partial Y}\right) + \frac{1}{Re}\left(\frac{\partial^2 U}{\partial X^2} + \frac{\partial^2 U}{\partial Y^2} - \frac{1}{Da}U\right)\right\} \tag{43}$$

The *Y*-momentum equation requires some adjustment with the addition of a new term. This term must be included as follows in the discretized equation, and the *Y*-momentum equation therefore assumes the form:

$$\bar{V} = V^n + dt\left[-\left(U\frac{\partial V}{\partial X} + V\frac{\partial V}{\partial Y}\right) + \frac{1}{Re}\left(\frac{\partial^2 V}{\partial X^2} + \frac{\partial^2 V}{\partial Y^2} - \frac{1}{Da}V\right) - \frac{Ha^2}{Re}V + Ri.\theta\right] \tag{44}$$

It is important to note that the temperature term T is co-located with velocity before being used in the previous equation to accommodate for the staggered grid. $\bar{U}$ and $\bar{V}$ are projected to obtain U and V using the following *Poisson pressure equation*:

$$\frac{\nabla^2 u^\circ}{dt} = \nabla^2 p \tag{45}$$

The discretized temperature equation can be obtained to compute θ at the next time level (θ^{n+1}) as follows:

$$\theta^{n+1} = \theta^n + \Delta t \left(- \left(U \frac{\partial \theta}{\partial X} + V \frac{\partial \theta}{\partial Y} \right) + \frac{1}{Re\,Pr} \left(\frac{\partial^2 \theta}{\partial X^2} + \frac{\partial^2 \theta}{\partial Y^2} + Q\theta \right) + \frac{Ha^2 Ec}{Re} V^2 + \right.$$

$$\left. \frac{Ec}{Re} \left(\frac{1}{Da} (U^2 + V^2) + \left(2 \left(\frac{\partial U}{\partial X} \right)^2 + 2 \left(\frac{\partial V}{\partial Y} \right)^2 + \left(\frac{\partial V}{\partial X} + \frac{\partial U}{\partial Y} \right)^2 \right) \right) \right) \quad (46)$$

4. Result and Discussion

The transport characteristics for unsteady, laminar, MHD, natural convective flow of $Cu/Al_2O_3 -$ water nanofluid inside a porous rectangular enclosure in the presence of viscous dissipation, Joule heating, and heat source/sink have been computed with the MAC method and the results are illustrated graphically in this section. The Maxwell and Brinkmann models are used to compute the effective thermal conductivity and viscosity of the considered nanofluids, as per the Tiwari-Das nanoscale formulation described earlier. The values of the dimensionless parameters, namely, the Reynolds number ($Re = 2\,\&\,10$), Prandtl number ($Pr = 7$), Richardson number ($0.01 \leq Ri \leq 100$), Hartmann number ($0 \leq Ha \leq 100$), Darcy number ($10^{-1} \leq Da \leq 10^{-3}$), volumetric heat generation/absorption coefficient ($-6 \leq Q \leq 6$), viscous dissipation and Joule heating parameter ($0 \leq Ec \leq 1$), and nanofluid volume fraction ($0 \leq \varphi \leq 0.05$) are considered based on previous studies [12,13,16,20,21,25,26]. Contour plots and graphs are presented in **Figs. 2- 13** to examine the impact of various pertinent parameters on streamlines, isotherms and local Nusselt number distributions and detailed physical interpretation of the obtained results is included.

4.1 Effects of Hartmann number on streamlines:

Figure 2 (A, B and C) shows the effect of Hartmann number on streamlines contours for Cu-water and Al₂O₃-water nanofluids. Hartmann number plays a significant role on the fluid flow and thermal convection process. It appears in the term, $- \left(\frac{\rho_f}{\rho_{nf}} \right) \left(\frac{\sigma_{nf}}{\sigma_f} \right) \frac{Ha^2}{Re} V$ in the secondary momentum Eqn. (19) since the applied magnetic field in the X-direction generates a Lorentzian magnetic body force perpendicular to the field which acts in the Y-direction. In the absence of a magnetic field ($Ha = 0$), the corresponding streamlines contours of both nanofluids show similar patterns as seen in Fig. 2A. However, the inner circulation cells of left eddies indicate a minor variation in the strength of streamlines of the Cu-water and Al₂O₃--water nanofluids. As the Hartmann number increases, the opposing Lorentz force is amplified. This magnetic body force is resistive (negative) and damps the flow. It therefore opposes the thermal buoyancy force (which is assistive and simulated with the term, $+ \frac{(\rho\beta)_{nf}}{\rho_{nf}\beta_f} Ri\,\theta$, also in Eqn.

(19). The shape and strength of the circulating eddies change noticeably as *Ha* increases. At lower *Ha* values there is a kidney-shaped structure to the single vortex on the left and right and each cell extends to the full depth of the enclosure. As magnetic field increases, this structure is broken, and 2 sets of double vortices are synthesized. This is due to the deceleration generated i. e. inhibiting effect of strong Lorentz drag force. Clearly therefore when *Ha = 50* and 100, the clockwise and anti-clockwise circular vortices have two eddies that rotate at the same speed but in opposite directions, creating the streamline contours as shown in Figs. 2B and 2C. This behaviour is further amplified for the final case where the maximum morphing in vortex cells corresponds to $Ha = 100$, for which the Lorentz magnetic drag force is 100 times the viscous hydrodynamic force, as demonstrated by vortices of the streamlines. Stronger magnetic field compresses the vortex cells in the vertical direction and expands them in the lateral direction. Momentum distribution in the regime is therefore significantly influenced with stronger magnetic field effect i. e. increment in Hartmann number. The *electrically non-conducting case (Ha = 0)* therefore produces a significantly different internal circulation compared to the magnetohydrodynamic cases (*Ha = 50, 100*). The implication is that substantial modification (damping) of the internal circulating flow can be achieved with strong transverse magnetic field which is very beneficial in materials processing operations, since the flow can be more effectively controlled to achieve different constitution of the electro-conductive nanomaterial.
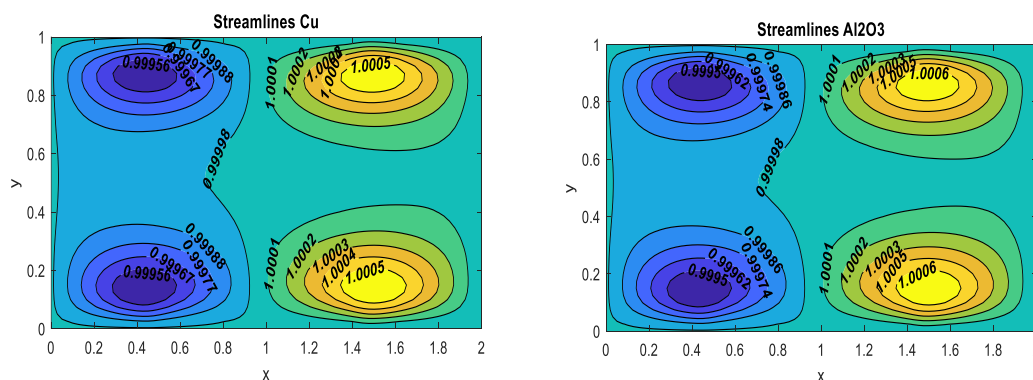
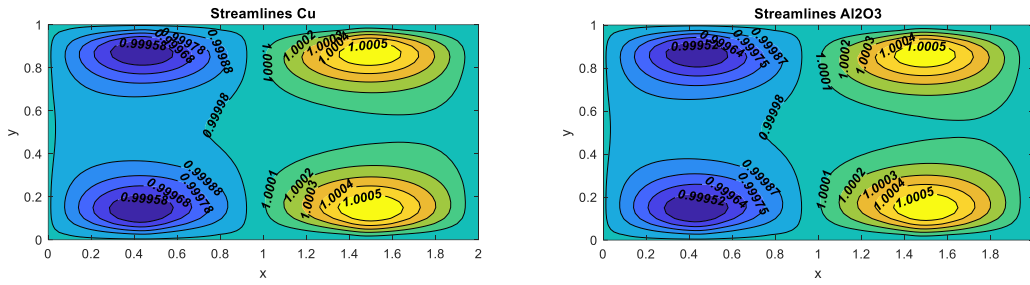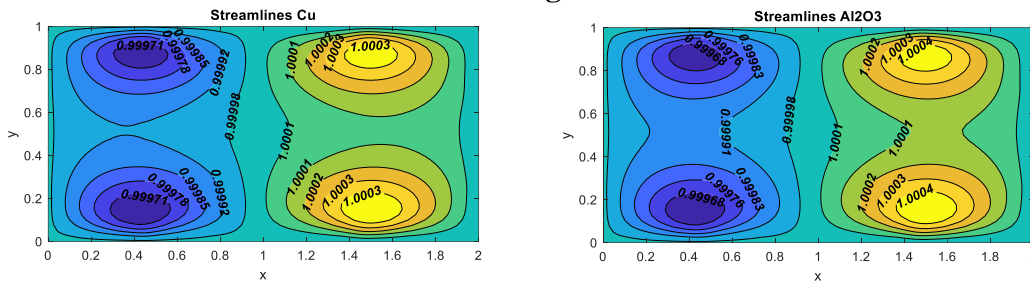## Figure A
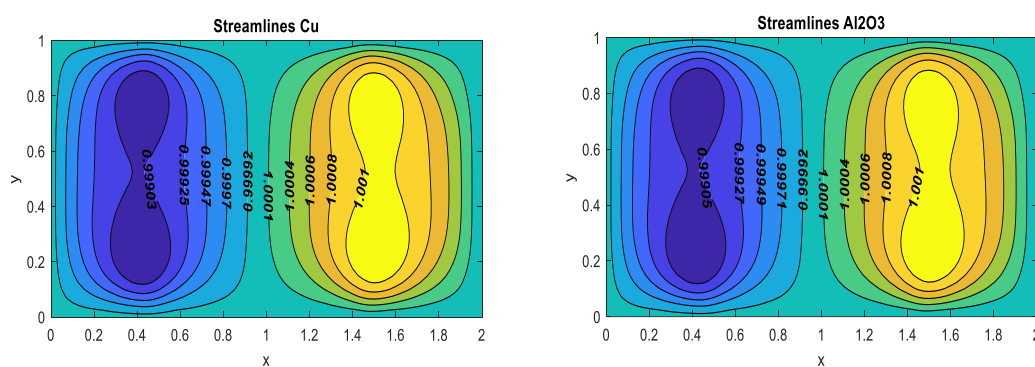
Figure B
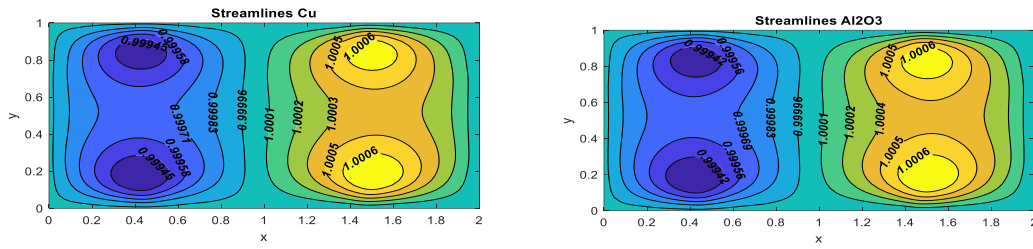
Figure C
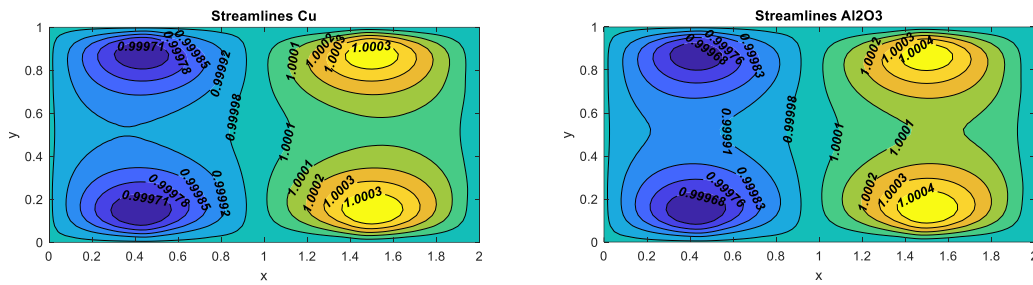
Figure 2: Streamlines for fixed values of $Da = 10^{-3}$; Hs=-6; φ =0.05; Ec=0.3; Ri=10; Pr=7; Re=10 and different values of *(A) Ha=0, (B) Ha=50, (C) Ha=100*

4.2 Effects of Darcy number on streamlines:

The presence of porous medium in any flow domain introduces solid matrix fibers dispersed throughout the regime. This matrix structure alters the fluid flow and associated heat transfer characteristics significantly. The porous medium permeability is symbolized here by permeability (K) which features in the Darcy number (Da). Darcy number arises in the primary and secondary momentum equations (18) and (19) in the linear Darcy drag force terms, viz, $-\left(\frac{v_{nf}}{v_f}\right)\frac{1}{Re\,Da}U$ and $-\left(\frac{v_{nf}}{v_f}\right)\frac{1}{Re\,Da}V$. These body forces are resistive and simulate the bulk matrix drag effect on the percolating magnetic nanofluid at low Reynolds number i.e. viscous-dominated flow. Figure 3 (A, B, and C) shows the streamline plots in the enclosure for variation of Darcy numbers ranging from 10^{-3} to 10^{-1}. These values correspond to a sparsely packed porous medium, representative of for example metallic foam. Enhancement in the permeability allow the nanofluid to flow more freely since more void space is available for percolation of the nanofluid. In this analysis, an increase in Da indicates an increase in permeability. When the Da value is very low, it indicates a lower permeability, which implies a higher resistance to the flowing fluid (magnification of the Darcian drag force terms explained previously, which are both *inversely proportional* to Da) and vice versa. As a result, the velocity of the flowing

fluid decreases for decreasing the Da values. At a lower Darcy value (Da = 10^{-3}), buoyancy-driven flow is significantly reduced, and thus the convective circulation is suppressed. Two sets of dual vortices are observed which are clustered near the upper and lower walls with a central gap (Figs. 3A). Figures 3A and 3B show that streamline contours for Cu-water and Al2O3-water nanofluids for $Da = 10^{-1}$ and 10^{-2}, respectively, are gradually broken into 2 eddies, with the shapes varying for both values of Da and nanoparticles. However, the right-hand side vortex pair are closer for the Al_2O_3-water nanofluid case (right plot) then the Cu-water case (left plot), especially near the right wall. In Fig. 3C these pairs of vortices start to merge in the vertical direction and the tendency is therefore to intensify the circulation at higher permeability. Considerable changes are therefore computed in the morphology at high Da (10^{-1}) value. Figure 3C also shows that different nanoparticles cause eddies to take different shapes inside the enclosure. The geometry is particularly modified for the Al_2O_3-water nanofluid case in the vicinity of the right wall of the enclosure, although changes are also apparent for the Cu-water case towards the central (core) zone. The presence of a porous medium therefore also offers an effective control mechanism for the internal circulation dynamics in the enclosure. Less permeable materials generate discrete dual vortex patterns in the left and right half space zones. More permeable materials produce a merging of the dual vortex cells and amplify the convective circulation in the cavity.

Figure A

Figure B

Figure C

Figure 3: Streamlines for fixed values of Ha=100, Hs=-6; φ =0.05; Ec=0.3; Ri=10; Pr=7; Re=10 and different values of (A) $Da = 10^{-1}$, (B) $Da = 10^{-2}$ (C) $Da = 10^{-3}$

4.3 Effects of heat source/sink on streamlines:

The effects of the heat source/sink parameter on the streamlines ($Q = Hs = -6, 0, 6$) are depicted in Fig. 4 (A, B, and C) for Cu-water and Al$_2$O$_3$-water nanofluids. The circulation in the core region is notably decreased for magnifying the internal heat generation. Further, as shown in Fig. 4, the density of the nanofluid near the hot wall increases as the hot portions and cool portions are located opposite to each other, and the nanofluid therefore moves upward along the horizontal wall. The density is decreased as the nanofluid reaches near the wall which contains cold portion, leading to a downward movement along the vertical wall which has hot portion again and reaching the wall with cold portion, so that a contour on the left and right side of the enclosure appears in the streamlines and their buoyancies are decomposed into two groups, which creates non-uniform contour curves in counter-clockwise and anti-clockwise directions set up by the hot on the right wall and left-side vertical walls in the enclosure. It is also noteworthy that with heat sink present i. e. Hs = -6, (Fig 4A) the Cu-water dual vortex structure near the left wall is impinging whereas it separates#, and the cells become more discrete for the absence of heat sink/source in Fig. 4(B) i. e. *Hs=0;* this trend is further amplified for the heat generation (source) case as observed in Fig. 4(C) i. e. *Hs=6.* The discrete dual cell structure is maintained at all values of *Hs* for the Al$_2$O$_3$-water nanofluid case, although the cells are progressively elongated in the lateral direction as the case changes from heat sink to heat source. The heat source/sink term, Q (defined as *Hs* in the plots) arises only in the energy conservation Eqn. (20) i. e. $\left(\frac{\alpha_{nf}}{\alpha_f}\right)\frac{Q}{Re\,Pr}\theta$. This term clearly energizes the flow when Q > 0 (heat source) whereas it de-energizes the flow when Q <0 (heat sink). This simple modification in the thermal field can therefore be exploited to strongly manipulate vortex cells structures in magnetic nanofluid filled porous enclosures, since there is strong coupling between the primary and secondary momentum equations (18), (19) via many terms including

the convective acceleration terms, $U \frac{\partial \theta}{\partial X} + V \frac{\partial \theta}{\partial Y}$ in Eqn. (20). The natural convection currents also imply a strong interplay between the temperature field and the velocity fields in the regime.
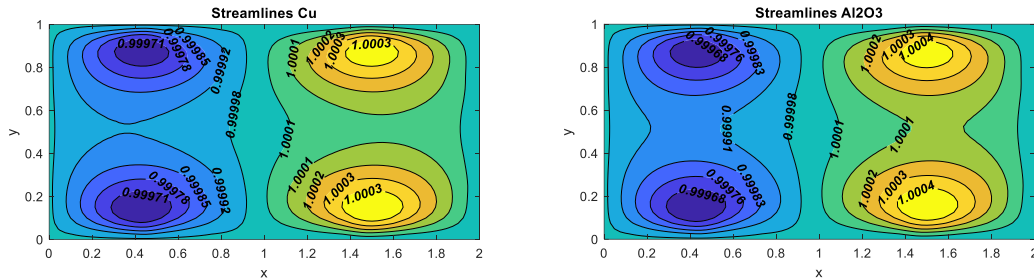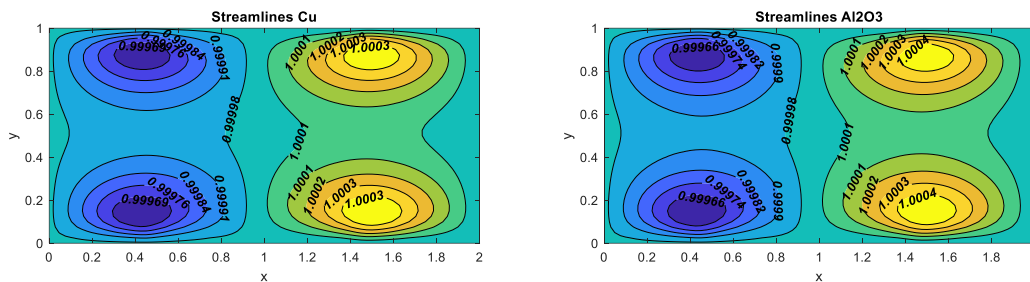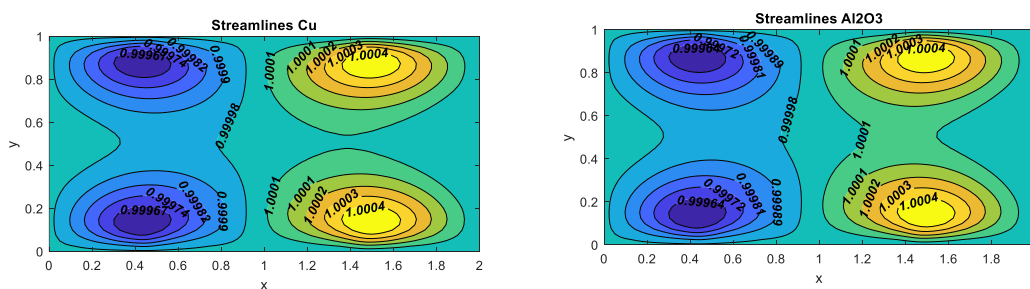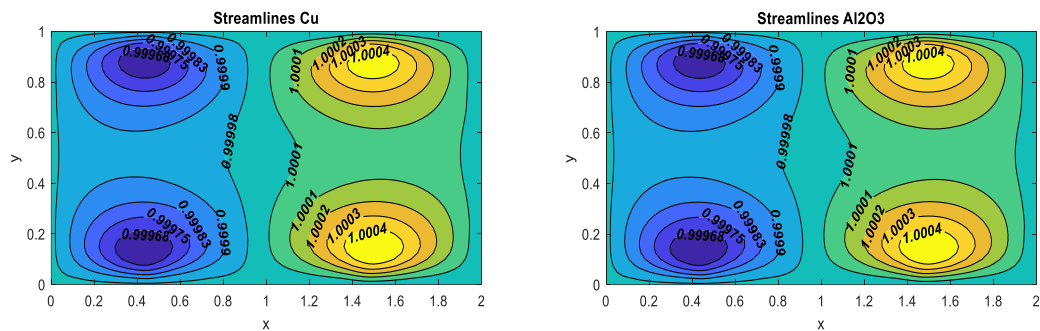
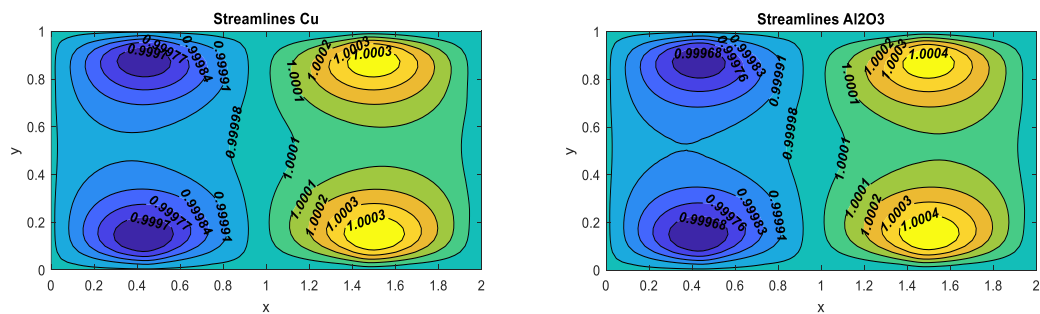**Figure A**

Figure B

Figure C

Figure 4: Streamlines for fixed values of $Da = 10^{-3}$; Ha=100; φ =0.05; Ec=0.3; Ri=10; Pr=7; Re=10 and different values of *(A) Hs=-6, (B) Hs=0, (C) Hs=6*

4.4 Effects of nanofluid volume fraction on streamlines:

Figure 5 (A, B, and C) depicts the effect of the volume fraction with variation between 0% and 5% of Cu and Al₂O₃ nanoparticles on the contours of streamlines in the rectangular enclosure. The flow structure in each phase is described by the presence of a clockwise and a

counterclockwise circulation of two different eddies (vortex cells) on the left and right sides of the enclosure. As seen in Fig. 5A, in the streamlines of $\varphi = 0$, the shape of the eddies for Cu-water and Al_2O_3-water nanofluids is somewhat different. Figure 5B depicts the changes in the left side eddy for both nanoparticles in the enclosure for $\varphi = 0.03$. Figure 5C portrays the drastic changes in the streamline vortex in the eddies for both nanoparticles when $\varphi = 0.05$. There are larger yellow zones in the Cu-water nanofluid case (left plots) corresponding to the higher thermal conductivity of copper nanoparticles. While similar yellow zones appear for the Al_2O_3-water nanofluid, they are more constrained at lower volume fractions and only expand for highest volume fraction (Fig. 5C). As volume fraction is increased, in Figs. 5B, C the dual vortex cells begin to impinge, and the trend is towards a merging o the two cells. This is strongly evident for the Al_2O_3-water nanofluid for Fig. (B) $\varphi=0.03$ but not for the Cu-water nanofluid case. However, for Fig. 5 (C) $\varphi=0.05$, the merging is achieved for both Cu-water and Al_2O_3-water nanofluid cases.
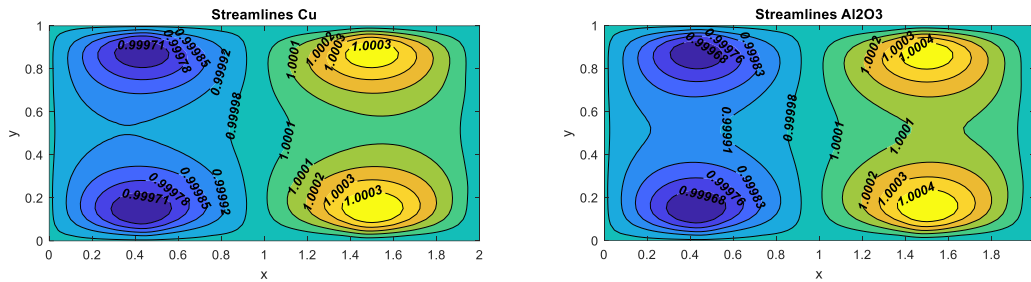
Figure A

Figure B

Figure C

Figure 5: Streamlines for fixed values of $Da = 10^{-3}$; Ha=100; Hs=-6; Ec=0.3; Ri=10; Pr=7; Re=10 and different values of (A) φ=0, (B) φ=0.03, (C) φ=0.05

4.5 Effects of Eckert number on streamlines:

The effect of the Eckert number with a variation between $0 \leq Ec \leq 1$ on the streamline contours of Cu-water and Al$_2$O$_3$-water nanofluids is shown in Figure 6 (A, B, and C). The eddies on the left and right sides of the enclosure are very different in shape and the eddies for Cu-water and Al$_2$O$_3$-water nanofluids also differ notably. There is a weak modification in in the shapes of the vortex cells (eddies) in Fig. 6 (A, B, and C) which represent the streamlines of Cu-water and Al$_2$O$_3$-water nanofluids. *Ec* features in both the viscous heating term in the energy Eqn. (20) and the Joule dissipation term i.e. $+ \left(\frac{\mu_{nf}}{\mu_f}\right) \left(\frac{(\rho C_p)_f}{(\rho C_p)_{nf}}\right) \frac{Ec}{Re} \left(2 \left(\frac{\partial U}{\partial X}\right)^2 + 2 \left(\frac{\partial V}{\partial Y}\right)^2 + \left(\frac{\partial V}{\partial X} + \frac{\partial U}{\partial Y}\right)^2\right)$ and $\left(\frac{\sigma_{nf}}{\sigma_f}\right) \left[\frac{(\rho C_p)_f}{(\rho C_p)_{nf}}\right] \frac{Ha^2 Ec}{Re} V^2$. Increment in *Ec* will dampen the internal flow since kinetic energy will be converted to heat. The streamlines are therefore relaxed with increasing Eckert number, since the momentum is inhibited in the regime. This leads to a relaxation in the core zone which is more evident in the Al$_2$O$_3$-water nanofluid than the Cu-water nanofluid case. However the dominant influence of Eckert number is on the isotherm distributions.
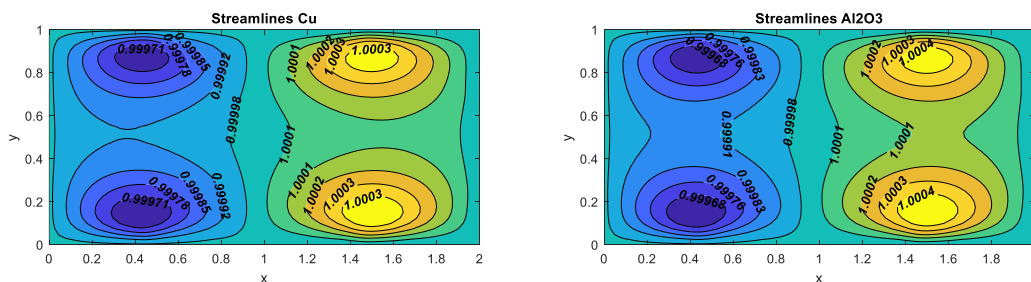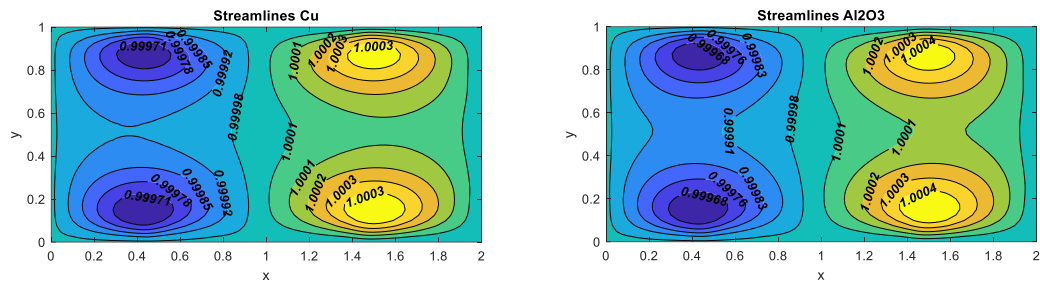
Figure A

Figure B
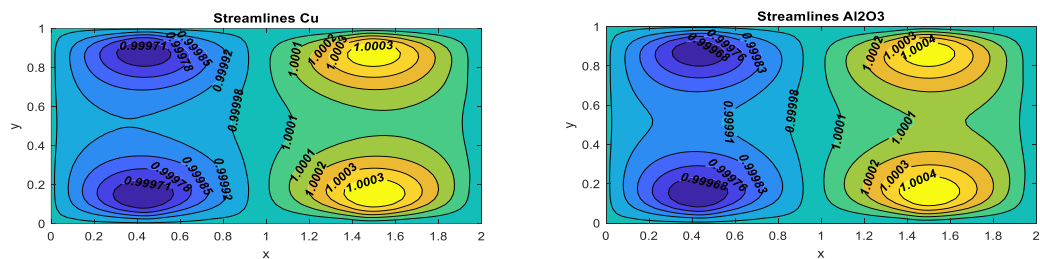

Figure C

Figure 6: Streamlines for fixed values of $Da = 10^{-3}$; Ha=100; φ=0.05; Hs=-6; Ri=10; Pr=7; Re=10 and different values of (A) Ec=0, (B) Ec=0.3, (C) Ec=1

4.6 Effects of Richardson number on streamlines:

To investigate the effect of the Richardson number (*Ri*) on nanofluid flow in the rectangular enclosure, the streamlines are presented in Fig. 7 (A, B, and C). Three different Richardson numbers ($Ri = 0.01, 1, 100$) are considered. The Richardson number plays an important role to determine the mode of convection. The convection mode is divided into three convective flow regimes, namely, *forced convection, mixed convection, and natural convection*, which are denoted by Ri<1, Ri=1, and Ri>1. *Ri* features in the single thermal buoyancy term, $+\frac{(\rho\beta)_{nf}}{\rho_{nf}\beta_f} Ri\, \theta$ in the secondary momentum equation (19). Figure 7(A) depicts two distinct eddies on the enclosure left and right sides at *Ri=0.01* and the shapes of the eddies for Cu-water and Al₂O₃-water nanofluids are noticeably different. When Ri is less than unity, the thermal buoyancy force has negligible effect. By increasing the value of Ri from 0.01 to 1, there are no changes in the shapes of the eddies, but the maximum value in contour changes for both Cu-water and Al₂O₃-water nanofluids. At Ri=1, neither forced nor natural convection takes priority and mixed convection is present in the enclosure. The shapes of eddies do not

change significantly when the Richardson number is increased to Ri=100 for both Cu-water and Al2O3-water nanofluids. However, the shapes of the eddies for all values of the Richardson number for both Cu-water and Al2O3-water nanofluids are significantly different; they are more laterally stretched for the former and more clustered for the latter.
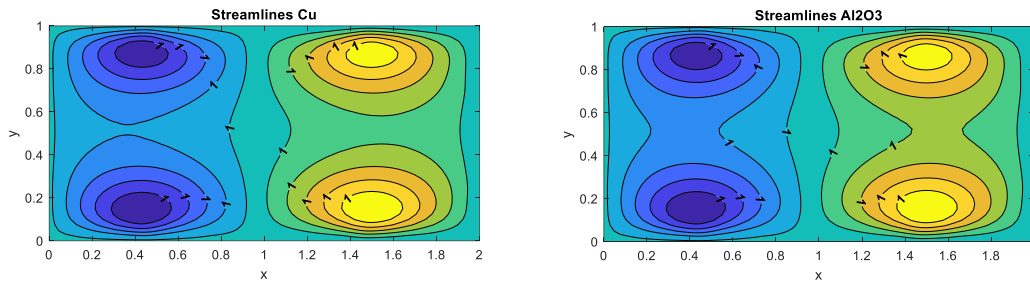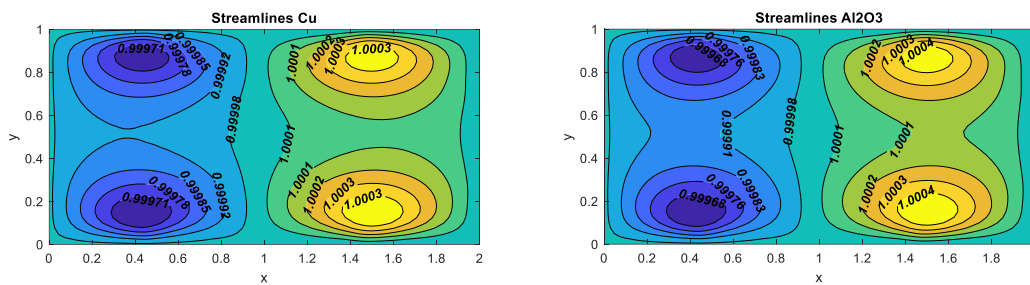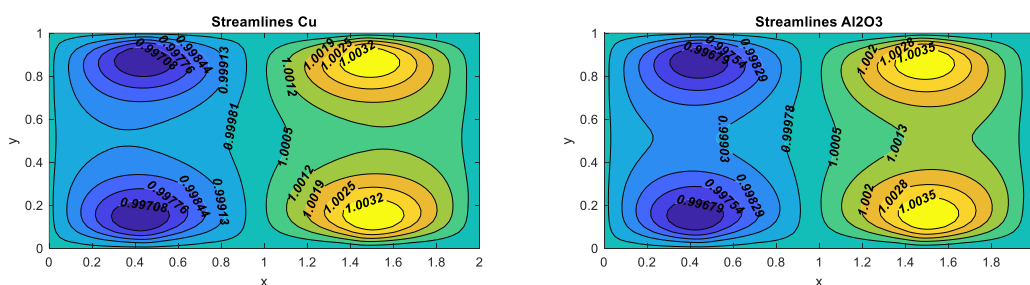
Figure A

Figure B

Figure C

Figure 7: Streamlines for fixed values of $Da = 10^{-3}$; Ha=100; φ=0.05; Hs=-6; Ec=0.3; Pr=7; Re=10 and different values of (A) Ri=0.01, (B) Ri=10, (C) Ri=100

4.7 Effects of heat source/sink on isotherms:

The temperature distribution inside the enclosure is considerably influenced by the heat source and sink parameter. As noted earlier, the heat source/sink term, Q (defined as Hs in the plots)

arises only in the energy conservation Eqn. (20) i. e. $\left(\frac{\alpha_{nf}}{\alpha_f}\right)\frac{Q}{Re\,Pr}\theta$. This term clearly energizes

the flow when $Q > 0$ (heat source) whereas it de-energizes the flow when $Q < 0$ (heat sink). In these simulations, the Reynolds number is constrained at $Re = 2$, for which the isotherm contours are very smooth and laminar. At the upper and lower horizontal walls, the blue contours indicate cooling in this vicinity and a strong reduction in heat transfer to these boundaries. With heat sink present (Fig. 8A) i. e. $Hs=-6$, there is a strong blue core central zone also for both nanofluids. However, in Fig. 8 (B) $Hs=0$ and Fig. 8(C) $Hs=6$ (heat generation), this cold blue central zone is eliminated and only the central sections of the top and lower base wall are cool. For the heat sink case (Fig 8A) there is a strong heat transfer intensity only on and near the left and right walls. However, in Figs. 8B, C the yellow warmer zones significantly extend into the enclosure and eventually merge creating a hot core zone. This is accompanied with significant distortion of the isotherms both in the core zone and also in proximity to the the left and right walls of the enclosure. The presence of a heat source ($Hs = 6$) clearly strongly energizes the regime and produces similar isotherm topologies for both nanofluids.
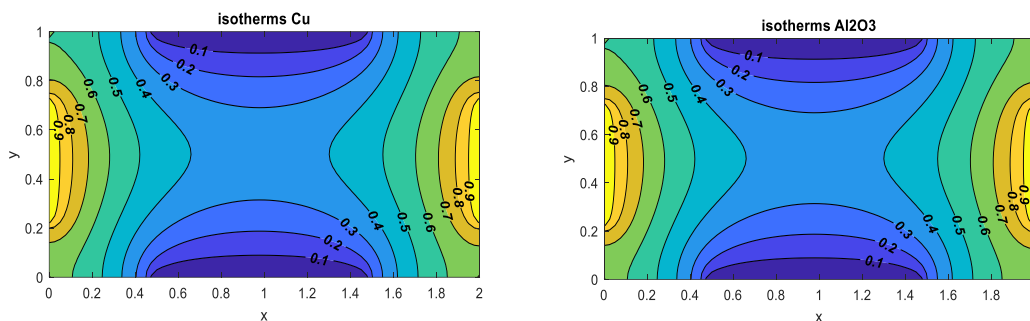
Figure A

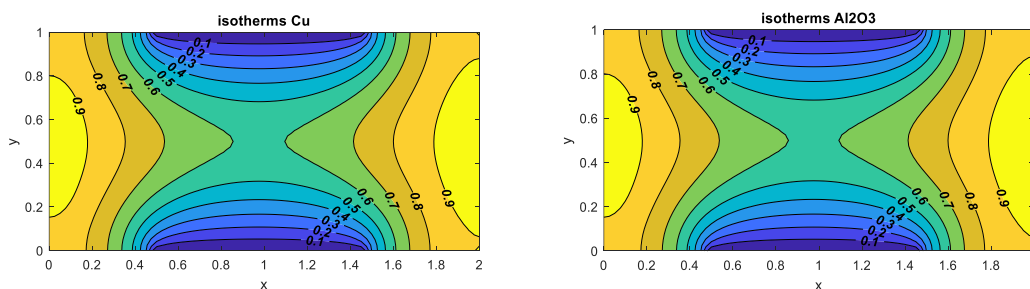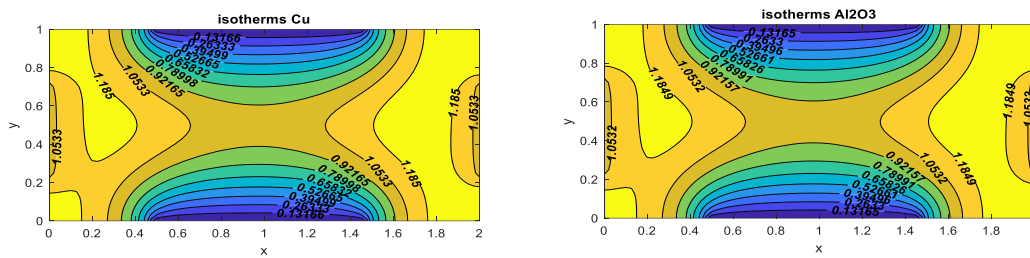**Figure B**

Figure C

Figure 8: Isotherms for fixed values of $Da = 10^{-3}$; Ha=100; φ =0.05; Ec=0.3; Ri=10; Pr=7; Re=2 and different values of (A) Hs=-6, (B) Hs=0, (C) Hs=6

4.8 Effects of nanofluid volume fraction on isotherms:

As shown in Figure 9, increased thermal conductivity produced with nanoparticle doping (volume fraction) generates denser isotherms. Therefore, increased natural convection, and heat transfer are induced on all sides of the enclosure. The heat transfer enhancement is due to the increased kinematic viscosity and thermal conductivity of the base fluid. This is further augmented with the presence of viscous dissipation and Joule heating effects and hence the temperature magnitudes are boosted. The yellow/green warmer zones are progressively expanded from the left and right walls and encroach deeper into the core zone with elevation in nanoparticles concentrations (0 to 5%). The distribution of isotherms therefore changes dramatically as the volume fraction increases. Nanoparticles have exceptional properties such as higher thermal conductivity and stability, which can improve energy transport capability. As a result, with the highest nanoparticle doping of the aqueous base fluid, more heat is transported into the fluid domain and thermal circulation is improved which is beneficial for fuel cell and also materials processing operations [31, 34, 36].
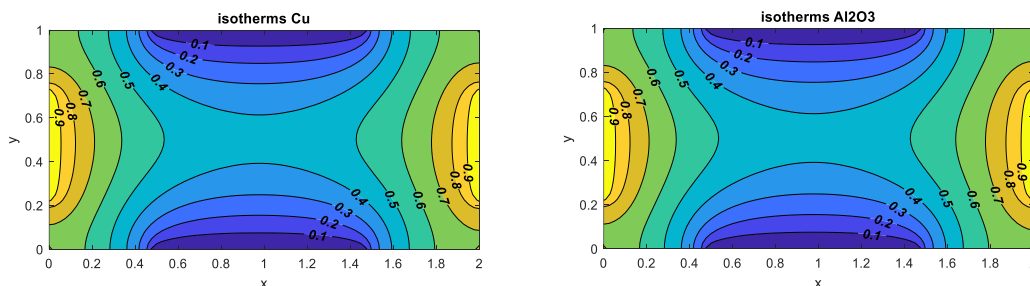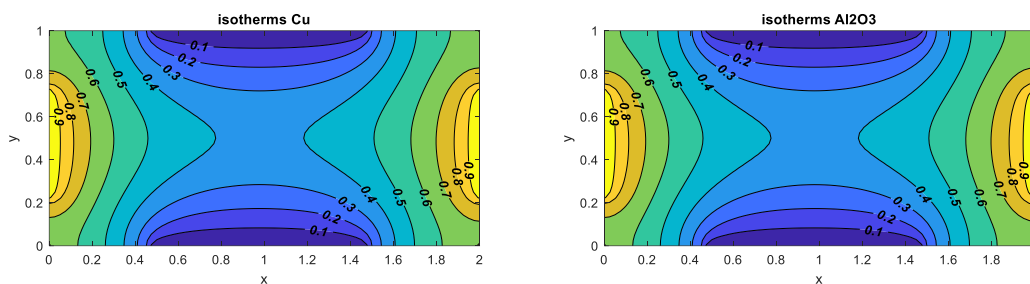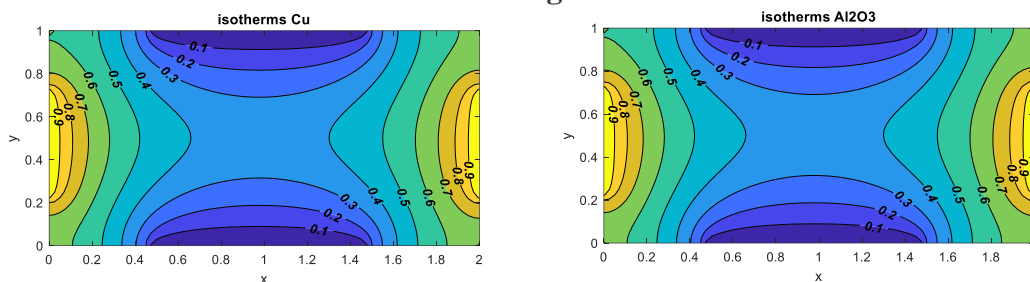
Figure A

Figure B

Figure C

Figure 9: Isotherms for fixed values of $Da = 10^{-3}$; Ha=100; Hs=-6; Ec=0.3; Ri=10; Pr=7; Re=2 and different values of (A) φ=0, (B) φ=0.03, (C) φ=0.05

4.9 Characteristics of Nusselt number distribution:

Fig. 10 illustrates the local Nusselt number along the base wall of the enclosure with *X* coordinate, for Cu-water nanofluid. An increase in the value of heat generation elevates the local Nusselt number whereas increasing heat sink reduces it. The presence of heat source (generation) heats the internal circulating fluid and mobilizes greater heat transfer to the lower wall (boundary). This boosts the Nusselt number. The opposite effect is induced for heat sink i. e. cooling of the base wall and suppression in temperatures of the internal nanofluid, resulting in a decrement in Nusselt number (reduced heat diffusion from the nanofluid to the base wall). It is seen that the local Nusselt number is concave upward in all three cases of heat absorption (*Hs* < 0), heat generation (*Hs* > 0), and without a heat source (i.e., *Hs* = 0). Fig. 11 shows the local Nusselt number profiles for Cu-water nanofluid with different volume fractions. It is noticed that the heat transfer rate increases with elevation in the volume fraction in the central location. The higher volume fraction presence (due to the high thermal conductivity of copper nanoparticles) assists in the transport of heat to the boundary. This elevates Nusselt number values particularly in the central region of the wall. Figure 12 shows the local Nusselt number for Al$_2$O$_3$-water nanofluid for heat generation/absorption parameter. An increase in the internal heat generation also notably increases the rate of heat transfer distribution whereas heat sink produces a depletion in Nusselt number, and again the effect is most prominent in the central

region of the base wall. Fig. 13 displays the local Nusselt number profiles for Al$_2$O$_3$-water nanofluid with different volume fractions. It is observed that the heat transfer rate weakly increases for magnifying the volume fraction. However, the reverse trend is observed at some places. The magnitudes are also significantly less than for the copper -water nanofluid case (see Fig. 11) since thermal conductivity of copper nanoparticles is superior to Al$_2$O$_3$ nanoparticles. Inspection of all the Nusselt graphs for both Cu-water and Al$_2$O$_3$-water nanofluids indicate that two sharp edges are present near the left and right walls, and a concave structure is present in the central section of the base wall.
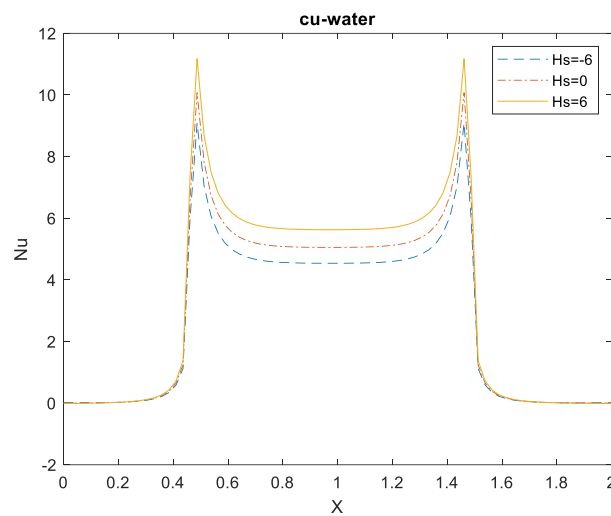

Figure 10: Nusselt number for fixed values of $Da = 10^{-3}$; Ha=100; φ =0.05; Ec=0.3; Ri=10; Pr=7; Re=10 and different values of Hs=-6, Hs=0, Hs=6

Figure 11: Nusselt number for fixed values of $Da = 10^{-3}$; Ha=100; Hs=-6; Ec=0.3; Ri=10; Pr=7; Re=10 and different values of φ=0, φ=0.03, φ=0.05

Figure 12: Nusselt number for fixed values of $Da = 10^{-3}$; Ha=100 φ =0.05; Ec=0.3; Ri=10; Pr=7; Re=2 and different values of Hs=-6, Hs=0, Hs=6

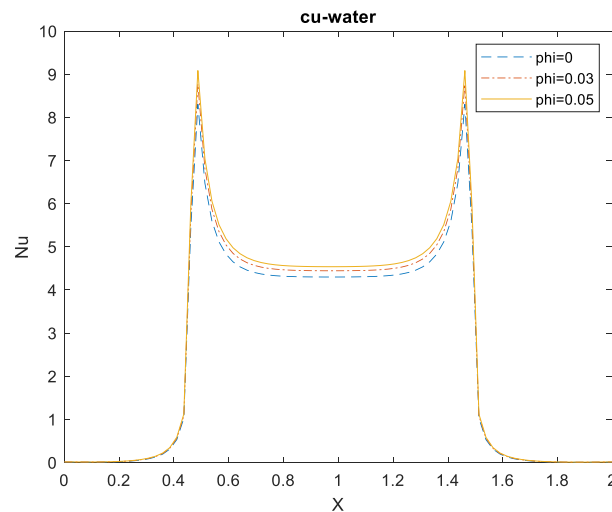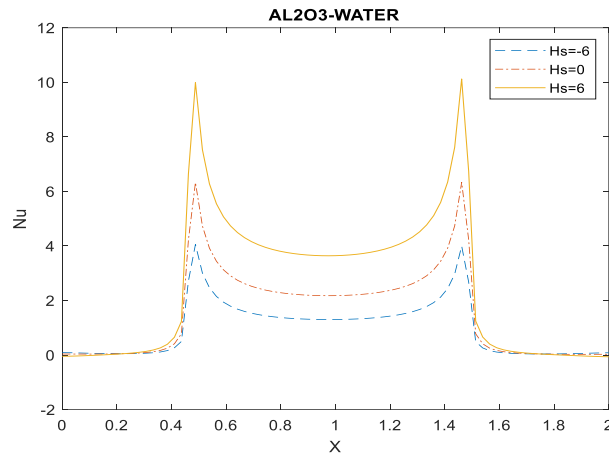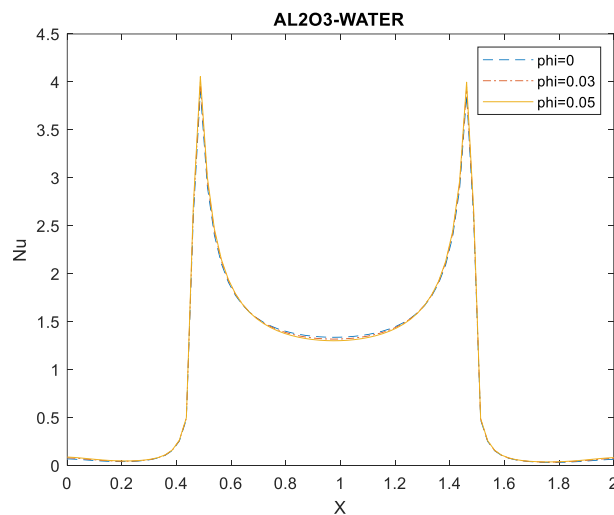**Figure 13:** Nusselt number for fixed values of $Da = 10^{-3}$; Ha=100; Hs=-6; Ec=0.3; Ri=10; Pr=7; Re=2 and different values of φ=0, φ=0.03, φ=0.05

5. Conclusions

In the present study, motivated by emerging applications in hybrid fuel cells and magnetic nano-materials processing technologies, a mathematical model has been developed to study the the conjugate effects of viscous dissipation and Joule heating on MHD natural convective flow of Cu- water and Al_2O_3-water nanofluids within a porous medium rectangular enclosure. A Tiwari-Das nanoscale model has been used which features Maxwell and Brinkman formulations for thermophysical properties of both nanofluids. A Darcian model has been adopted for the porous medium drag force effects at low Reynolds number. The enclosure top and bottom walls have cool portions, while the left and right walls have hot portions. Except for the middle portions, the walls of the enclosure are adiabatic. Numerical solutions of the transformed dimensionless conservation equations with appropriate boundary conditions have

been obtained with the accurate, stable, finite difference marker and cell (MAC) method. The key observations of the simulations may be summarized below:

- With an increase in the volume fraction of either copper or alumina nanoparticles, the flow circulation (streamline magnitudes) and isotherm values of the magnetic nanofluid inside the rectangular enclosure are increased.

- Greater doping of base fluid (water) with either copper or alumina solid nanoparticles increases the temperatures, although copper performs better.

- The permeability of porous media plays an important role in the convective heat transfer characteristics. The resistance to fluid flow decreases as the value of the Darcy number increases. This increases the rate of heat transfer and also intensifies circulation in the enclosure (flow acceleration).

- Internal heat generation (source) increases the isotherm magnitudes whereas heat absorption (sink) depletes them.

- The shapes of the vortex cells (eddies) for all values of the Richardson number for both Cu-water and Al_2O_3-water nanofluids are significantly different; they are more laterally stretched for the former and more clustered for the latter.

- Increment in *Eckert number (dissipation) parameter* dampens the internal flow since kinetic energy is increasingly converted to thermal energy (heat). This amplifies both viscous heating and Joule (magnetic) heating effects and results in a relaxation in streamlines in the core zone due to momentum being inhibited in the regime. The relaxation in the core zone is more evident in the Al_2O_3-water nanofluid than the Cu-water nanofluid case.

- The shape and strength of the circulating eddies is strongly modified with increasing Hartmann number (magnetic field parameter). At lower *Ha* values there is a kidney-shaped structure to the single vortex on the left and right, and each cell extends to the full depth of the enclosure. As magnetic field increases, this structure is broken, and 2 sets of double vortices are synthesized. This is due to the deceleration generated i. e. inhibiting effect of strong Lorentz drag force. Stronger magnetic field compresses the vortex cells in the vertical direction and expands them in the lateral direction.

- Richardson number and volume fractions have a greater impact on heat transfer enhancement in assisting flows than in opposing flows.

- Magnetic field, porous media and heat source/sink effects provide excellent mechanisms for modifying thermal/fluid transport characteristics in enclosure nanofluid dynamics.

The present investigation has revealed some intriguing characteristics of magnetohydrodynamic nanofluid convection in enclosures using different metallic nanoparticles. The MAC algorithm has been shown to be very accurate and versatile for simulating such problems of relevance to hybrid magnetic nano-fuel cells and materials processing operations. However, attention has been confined to Newtonian nanofluids. Future studies may extend the present analysis, to include non-Newtonian nanofluid characteristics e.g. viscoplastic, viscoelastic and microstructural (couple stresses). Efforts in this direction are currently underway and will be communicated soon.

References

[1]. Hussain CM, editor. *Handbook of Nanomaterials for Industrial Applications*. Elsevier; 2018 Jul 19.

[2]. Sivaraj R, Banerjee S. Transport properties of non-Newtonian nanofluids and applications. *The European Physical Journal Special Topics*. 2021 May 21:1-5.

[3]. Kavitha R, Abd Algani YM, Kulkarni K, Gupta MK. Heat transfer enhancement in a double pipe heat exchanger with copper oxide nanofluid: An experimental study. *Materials Today: Proceedings*. 2021 Nov 20.

[4]. B.A.I. Bendrer, A. Abderrahmane, S. E. Ahmed, Z. A.S. Raizah, 3D magnetic buoyancy-driven flow of hybrid nanofluids confined wavy cubic enclosures including multi-layers and heated obstacle, *International Communications in Heat and Mass Transfer* 126 (2021) 105431.

[5]. Sheikholeslami M, Gorji-Bandpy M, Vajravelu K. Lattice Boltzmann simulation of magnetohydrodynamic natural convection heat transfer of Al2O3–water nanofluid in a horizontal cylindrical enclosure with an inner triangular cylinder. *International Journalf Heat Mass Transfer*. 2015 Jan 1; 80:16-25.

[6]. Javed T, Mehmood Z, Siddiqui MA, Pop I. Effects of uniform magnetic field on the natural convection of Cu–water nanofluid in a triangular cavity. *International Journal Numerical Methods Heat & Fluid Flow*. 2017 Feb 6.

[7]. Balla CS, Kishan N, Gorla RS, Gireesha BJ. MHD boundary layer flow and heat transfer in an inclined porous square cavity filled with nanofluids. *Ain Shams Engineering Journal.* 2017 Jun 1;8(2):237-54.

[8]. Sheikholeslami M. *Application of control volume based finite element method (CVFEM) for nanofluid flow and heat transfer*. Elsevier; USA (2019).

[9]. P. Nithiarasu, K.N. Seetharamu, T. Sundararajan, Natural convective heat transfer in a fluid saturated variable porosity medium, *Int. J. Heat Mass Transfer* 40 (16) (1997) 3955–3967.

[10]. Mansour MA, Ahmed SE, Chamkha AJ. Entropy generation optimization for MHD natural convection of a nanofluid in porous media-filled enclosure with active parts and viscous dissipation. *International Journal of Numerical Methods for Heat & Fluid Flow*. 2017 Feb 6.

[11]. Reddy ES, Panda S. MHD natural convection nanofluid flows in a wavy trapezoidal porous enclosure with differentially heated side walls. *Journal of the National Science Foundation of Sri Lanka.* 2020;48(1)

[12]. Sajjadi H, Delouei AA, Mohebbi R, Izadi M, Succi S. Natural convection heat transfer in a porous cavity with sinusoidal temperature distribution using Cu/water nanofluid: Double MRT lattice Boltzmann method. *Commun. Comput. Phys*. 2021 1;29(1):292-318.

[13]. Al-Farhany K, Al-Chlaihawi KK, Al-dawody MF, Biswas N, Chamkha AJ. Effects of fins on magnetohydrodynamic conjugate natural convection in a nanofluid-saturated porous inclined enclosure. *International Communications in Heat and Mass Transfer.* 2021; 126:105413.

[14]. Badruddin IA, Zainal ZA, Narayana PA, Seetharamu KN. Heat transfer in porous cavity under the influence of radiation and viscous dissipation. *International Communications in Heat and Mass Transfer*. 2006; 33(4):491-9.

[15]. Hossain A, Gorla RS. Effect of viscous dissipation on mixed convection flow of water near its density maximum in a rectangular enclosure with isothermal wall. *International Journal of Numerical Methods for Heat & Fluid Flow*. 2006.

[16]. Sheikholeslami M, Hayat T, Alsaedi A. MHD free convection of Al_2O_3–water nanofluid considering thermal radiation: a numerical study. *International Journal of Heat and Mass Transfer.* 2016; 96:513-24.

[17]. Ghalambaz M, Sabour M, Pop I. Free convection in a square cavity filled by a porous medium saturated by a nanofluid: viscous dissipation and radiation effects. *Engineering Science and Technology, An International Journal.* 2016, 19(3):1244-53.

[18]. Swain BK, Parida BC, Kar S, Senapati N. Viscous dissipation and Joule heating effect on MHD flow and heat transfer past a stretching sheet embedded in a porous medium. *Heliyon*. 2020;6(10): e05338.

[19]. Rahman MM, Alim MA, Sarker MM. Numerical study on the conjugate effect of Joule heating and magneto-hydrodynamics mixed convection in an obstructed lid-driven square cavity. *International Communications in Heat and Mass Transfer*. 2010 1;37(5):524-34.

[20]. Mehmood K, Hussain S, Sagheer M. Mixed convection in alumina-water nanofluid filled lid-driven square cavity with an isothermally heated square blockage inside with magnetic field effect: *International Journal of Heat and Mass Transfer*. 2017; 109:397-409.

[21]. Dutta S, Bhattacharyya S, Pop I. Nonhomogeneous model for conjugate mixed convection of nanofluid and entropy generation in an enclosure in presence of inclined magnetic field with Joule heating. *International Journal of Numerical Methods for Heat & Fluid Flow*. 2020 Jul 16.

[22]. Khan MR, Mao S, Deebani W, Elsiddieg AM. Numerical analysis of heat transfer and friction drag relating to the effect of Joule heating, viscous dissipation and heat generation/absorption in aligned MHD slip flow of a nanofluid. *International Communications in Heat and Mass Transfer.* 2022; 131:105843.

[23]. Kumar BR, Sivaraj R. Heat and mass transfer in MHD viscoelastic fluid flow over a vertical cone and flat plate with variable viscosity. *International Journal of Heat and Mass Transfer.* 2013;56(1-2):370-9.

[24]. Prakash J, Kumar BR, Sivaraj R. Radiation and Dufour effects on unsteady MHD mixed convective flow in an accelerated vertical wavy plate with varying temperature and mass diffusion. *Walailak Journal of Science and Technology (WJST).* 2014;11(11):939-54.

[25]. Mythili D. and R. Sivaraj, M.M. Rashidi, Heat generating/absorbing and chemically reacting Casson fluid flow over a vertical cone and flat plate saturated with non-Darcy porous medium, *International Journal of Numerical Methods for Heat and Fluid Flow* 27 (2017) 156-173.

[26]. Hussain S, Öztop HF, Mehmood K, Abu-Hamdeh N. Effects of inclined magnetic field on mixed convection in a nanofluid filled double lid-driven cavity with volumetric heat generation or absorption using finite element method. *Chinese Journal Physics*. 2018;56(2):484-501.

[27]. Sivasankaran S, Alsabery AI, Hashim I. Internal heat generation effect on transient natural convection in a nanofluid-saturated local thermal non-equilibrium porous

inclined cavity. *Physica A: Statistical Mechanics and Its Applications*. 2018; 509:275-93.

[28]. Tayebi T, Öztop HF, Chamkha AJ. Natural convection and entropy production in hybrid nanofluid filled-annular elliptical cavity with internal heat generation or absorption. *Thermal Science and Engineering Progress*. 2020; 19:100605.

[29]. R.J. Tiwari, M.K. Das, Heat transfer augmentation in a two-sided lid-driven differentially heated square cavity utilizing nanofluids, *Int. J. Heat. Mass Transf.,* 50 (2007), pp. 2002-2018.

[30]. K. Venkatadri, O. Anwar Bég, P. Rajarajsweri and V. R. Prasad, Numerical simulation of thermal radiation influence on natural convection in a trapezoidal enclosure: heat flow visualization through energy flux vectors, *Int. J. Mechanical Sciences* (2019). doi.org/10.1016/j.ijmecsci.2019.105391 (9 pages)

[31]. O. Anwar Bég, K. Venkatadri, V.R. Prasad, T. A. Bég, A. Kadir and Henry J. Leonard, Numerical simulation of hydromagnetic Marangoni convection flow in a Darcian porous semiconductor melt enclosure with buoyancy and heat generation effects, *Materials Science and Engineering B: Advanced Functional and Solid-State Materials,* 261, (2020) 114722. (23 pages)

[32]. S. Kuharat, O. Anwar Bég, Ali Kadir and B. Vasu, Computation of metallic nanofluid natural convection in a two-dimensional solar enclosure with radiative heat transfer, aspect ratio and volume fraction effects, *Arabian J. Science and Engineering* (2020). (19 pages). doi.org/10.1007/s13369-020-04678-1

[33]. Sheikholeslami M, Mahian O. Enhancement of PCM solidification using inorganic nanoparticles and an external magnetic field with application in energy storage systems. *J Clean Prod.* (2019) 215:963–77.

[34]. Sireetorn Kuharat, O. Anwar Bég, Ali Kadir, B. Vasu, Tasveer A. Bég and W.S. Jouri, Computation of gold-water nanofluid natural convection in a three-dimensional tilted prismatic solar enclosure with aspect ratio and volume fraction effects, *Nanoscience and Technology- An International Journal,* 11(2):141–167 (2020).

[35]. W. Al-Kouz, A. Abderrahmane, M. Shamshuddin, O. Younis, S. Mohammed, O. Anwar Bég, D. Toghraie, Heat transfer and entropy generation analysis of water-Fe_3O_4/CNT hybrid magnetic nanofluid flow in a trapezoidal wavy enclosure containing porous media with the Galerkin finite element method, *European Physical Journal Plus* (2021). 136:1184 https://doi.org/10.1140/epjp/ s13360-021-02192-3 (23 pages)

[36].   W. Al-Kouz *et al.,* Effect of a rotating cylinder on the 3D MHD mixed convection in a phase change material filled cubic enclosure, *Sustainable Energy Technologies and Assessments,* 51 (2022) 101879.

[37].   Y Cao *et al.,* MHD natural convection nanofluid flow in a heat exchanger: Effects of Brownian motion and thermophoresis for nanoparticles distribution, *Case Studies in Thermal Engineering,* 28 (2021) 101394.